International Journal of Pharmaceutics 369 (2009) 185–195

Contents lists available at ScienceDirect

International Journal of Pharmaceutics

journal homepage: www.elsevier.com/locate/ijpharm

Pharmaceutical Nanotechnology

Characteristics and properties of nanospheres co-loaded with lipophilic and hydrophilic drug models

T. Hammady[a], A. El-Gindy[b], E. Lejmi[a], R.S. Dhanikula[a], P. Moreau[a,c], P. Hildgen[a,c,*]

[a] Faculté de pharmacie, Université de Montréal, Canada
[b] Faculty of Pharmacy, University of Suez Canal, Egypt
[c] Groupe de Recherche Universitaire sur le Médicament funded by Fonds de la recherche en santé du Québec (FRSQ), Canada

ARTICLE INFO

Article history:
Received 15 July 2008
Received in revised form 21 October 2008
Accepted 28 October 2008
Available online 17 November 2008

Keywords:
Co-encapsulation
Lipophilic
Hydrophilic
Derivative spectrophotometry
Microemulsion
Multiblock copolymer

ABSTRACT

The biphasic nature of polymeric nanospheres prepared by the double emulsion method was exploited to co-encapsulate lipophilic and hydrophilic molecules. All-trans retinoic acid (RA) was selected as a lipophilic drug model whereas calf thymus DNA was chosen as a water-soluble model. Simultaneous quantification of the loaded ingredients was achieved by a second derivative spectrophotometric technique. In addition, prepared batches were fully characterized by atomic force microscopy, porosity measurement, and thermal analysis. Finally, the angiosuppressive action of loaded RA was assessed in a tissue culture model. A blend of either polycaprolactone-multiblock copolymer or the microemulsion technique improved DNA-loading, whereas RA-loading was decreased. DSC data were helpful in explaining the initial phase of RA release from the nanospheres. Along with affinity for the polymeric matrix, the microporosity of nanospheres seemed to play an important role in the diffusion rate and release profiles of both loaded drug models in aqueous medium. The anti-angiogenic effect of microencapsulated RA was generally more pronounced than that of the free drug, and its inhibitory action was maintained for the 14-day study period. Moreover, a relationship was observed between the release profiles and anti-angiogenic properties of the batches tested.

1. Introduction

The combined therapy approach is attracting growing interest because of its proven efficacy against many diseases, such as malignant tumours, type 2 diabetes (Stafford and Elasy, 2007), cardiovascular maladies (Bakris, 2008), and autoimmune disorders (Strober and Clarke, 2004). In this respect, it would be beneficial to develop drug delivery systems that have the potential to transport more than one medication. In the field of pharmaceutical technology, polymeric nanoparticulate carriers made from polyesters possess many advantages, such as biocompatibility, biodegradability, long-term drug release and the possibility of drug targeting (Brigger et al., 2002; Panyam and Labhasetwar, 2003; Sunderland et al., 2006). Developed mainly to deliver hydrophilic drugs, micro/nanospheres prepared by multiple emulsion solvent evaporation consist of an aqueous phase embedded in a polymeric matrix (Blanco and Alonso, 1997; Iwata et al., 1999). Their unique structure makes it possible to co-encapsulate two different drugs, a lipophilic molecule that may be incorporated in the polymeric matrix, and a hydrophilic agent that may be dissolved in the embedded aqueous phase (Hombreiro Pérez et al., 2000). Such an approach may provide opportunities to apply combined therapy strategies via a common nanoparticular carrier.

Whenever drug co-encapsulation is required, it should be noted that a highly hydrophobic polymer is more likely to enhance encapsulation of the more lipophilic drug (Dong and Bodmeier, 2006), whereas the introduction of a hydrophilic moiety in the backbone of the polyester polymer has been shown to improve its ability to retain a hydrophilic molecule. This most probably occurs by virtue of stabilization of primary water in oil (w/o) emulsion during the preparation of microparticles by the double emulsion method (Yang et al., 2001). In this respect, application of the microemulsification concept to enhance the stability of the primary emulsion raises the loading efficiency of DNA in nanospheres produced by the mentioned technique (Hammady et al., 2006).

All-trans retinoic acid (RA) is a highly lipophilic molecule possessing interesting angiosuppressive and anti-cancer activity that has intrigued many workers (Lin et al., 2005; Chansri et al., 2008). However, its clinical application is limited by rapid liver metabolism and a short biological half-life (Muindi et al., 1992). In addition,

* Corresponding author at: Faculté de pharmacie, Université de Montréal, C.P. 6128, Succursale Centre-ville, Montréal, Québec, Canada H3C 3J7.
Tel.: +1 514 343 6448; fax: +1 514 343 6871.
E-mail address: patrice.hildgen@umontreal.ca (P. Hildgen).

0378-5173/$ – see front matter © 2008 Elsevier B.V. All rights reserved.
doi:10.1016/j.ijpharm.2008.10.034

RA is a very unstable molecule, especially in the presence of light and oxygen, where its degradation pathways include oxidation, isomerization, and photolysis (Tashtoush et al., 2008). For all these reasons, RA represents a challenging drug model for microencapsulation studies in which the main aim is to enhance its therapeutic effectiveness over an extended period of time (Jenning and Golan, 2001; Ioele et al., 2005; Choi et al., 2006).

Along with RA, we chose calf thymus DNA as a hydrophilic macromolecule model for co-loading in biphasic nanospheres prepared by the water in oil in water (w/o/w) double-emulsion, solvent evaporation method. Such a fragile hydrosoluble molecule can be representative of many recombinant macromolecules with therapeutic value, such as peptides, proteins, and plasmid DNA (Lengsfeld et al., 2002; Hammady et al., 2006; Degim and Celebi, 2007). Different batches of nanospheres loaded with both DNA and RA were prepared in an attempt to optimize the encapsulation efficiencies of the two model molecules. Simultaneous quantification of the loaded ingredients in each preparation was achieved by means of second derivative spectrophotometry (El-Gindy et al., 2001), while derivative spectrophotometry was associated with spectrofluorometry to assess both ingredients in release studies. The main purpose of this work was to obtain and characterize nanospheres co-loaded with two drug models despite their opposite hydro/lipophilic characteristics.

2. Materials and methods

2.1. Materials

Polylactide (PLA) (M_W 50,000) and poly(D,L-lactide)-*b*-poly(ethyleneglycol) multiblock copolymer $(PLA\text{-}PEG\text{-}PLA)_n$ (M_W 16,000) were synthesized in our laboratory (Quesnel and Hildgen, 2005). Calf thymus DNA, as sodium salt, RA, and Tris–EDTA buffer were purchased from Sigma–Aldrich (St. Louis, MO, USA). Polycaprolactone (PCL) (M_W 25,000) and polyvinyl alcohol (PVA) (M_W 9000–10,000, 80% hydrolyzed) were obtained from the Aldrich Chemical Company, Inc. (Milwaukee, WI, USA), whereas Span 80 was supplied by Fluka (St. Louis, MO, USA). All organic solvents were of analytical grade and supplied by Laboratoire MAT (Montreal, QC, Canada).

2.2. Tissue culture media and reagents

Normalized media and fetal calf serum were bought from Gibco (Burlington, ON, Canada) whereas growth supplements and insulin were procured from the Sigma Chemical Co. (St. Louis, MO, USA).

2.3. Preparation of nanospheres

Nanospheres were prepared by an adapted (w/o/w) double-emulsion, solvent diffusion technique (Hammady et al., 2006). Briefly, the organic phase consisted of 0.5 g of the polymer (or polymer blend) and an accurately weighed amount of the lipophilic ingredient, RA, dissolved in 10 mL dichloromethane. A calculated amount of Span 80 (0.4%, w/v), either associated or not with n-butanol as co-surfactant, was incorporated in the organic phase.

The w/o/w double emulsion was prepared by a two-step emulsification procedure. The primary (w/o) emulsion was obtained by dispersing 500 μL of aqueous DNA solution in the previously described organic phase, and by vortexing for 1 min, followed by 30-s homogenization with a high-speed turbo stirrer. The primary w/o emulsion was then gently syringed into 100 mL of 0.5% (w/v) PVA aqueous solution containing 10% (w/v) sucrose, for high-pressure homogenization (Emulsiflex C30, Avestin, Ottawa, ON, Canada) at 10,000 psi for 3 min to obtain multiple w/o/w emulsions. The volumes of the latter were adjusted to 250 mL with the external aqueous phase, then stirred for 5 h under reduced pressure to allow extraction and, eventually, evaporation of the organic solvent(s) with subsequent hardening of the nanospheres. The prepared nanospheres were washed by five successive ultracentrifugation/redispersion cycles in deionized water at 41,340 × *g* for 1 h each at 4 °C (Sorvall Evolution, Kendro Laboratory Products, Newtown, CT, USA), dried by lyophilization and stored at −4 °C until further investigation. Batch names along with the variable parameters used for the preparation of every batch are presented in Table 1.

2.4. Second derivative spectrophotometry (^2D)

Stock solutions were prepared by dissolving RA(I) in methanol and DNA(II) in sterile 0.1 M phosphate buffer saline (PBS). Standard solutions were obtained by dilution of stock solutions with sterile PBS to reach concentration ranges of 0.125–1.25 μg mL^{-1} (in 0.125-μg increments, $n = 10$) and 5–50 μg mL^{-1} (in 5-μg increments, $n = 10$) for I and II, respectively. Working standard solutions of DNA and RA mixtures in PBS were prepared as well from stock solutions, at concentration ratios (DNA to RA) ranging from 1:0.0012 to 1:0.03.

The second-order derivative spectra (^2D) of aqueous PBS working standard solutions containing varying amounts of each ingredient and those containing mixtures of both ingredients were scanned in the 500–200 nm range against PBS as blank. Calibration curves using ^2D for both agents were constructed and validated for analytical data and regression characteristics. The accuracy of the modified ^2D method was checked by analyzing seven synthetic mixtures of I and II at various concentrations within their respective linearity ranges, at concentration ratios (I:II) ranging from 1:0.0012 to 1:0.03.

In the course of encapsulation efficiency (EE) and drug release studies, control experiments were run on empty nanospheres in parallel to those performed on loaded nanospheres. Aliquots taken from control experiments served as blank solutions during the analysis of their corresponding test samples.

2.5. Differential scanning calorimetry (DSC) measurements of RA in nanospheres

The thermal properties of RA residues in prepared nanosphere batches were studied by DSC analysis (DSC Q1000, V9.0, build 275, Universal 4.1 D, TA Instruments, New Castle, DE, USA). Briefly, 2–5 mg of each sample were accurately weighed, then sealed in crimped aluminum pans with lids, and heated at a rate of 10 °C/min, from −40 to 250 °C. The samples were purged with pure, dry nitrogen at a flow rate of 50 mL/min. DSC was calibrated for temperature with indium (Goodfellow, 99.999% pure) and tin (NIST SRM 2000). Pure RA and blank nanospheres were similarly examined.

2.6. Atomic force microscopy (AFM) of nanospheres

AFM was performed with Nanoscope IIIa, Dimension™ 3100 (Digital Instruments, Santa Barbara, CA, USA) in tapping mode. Samples were prepared by suspending the nanoparticles in water at a concentration of 10 mg/mL. The samples were deposited on a freshly cleaved mica surface and allowed to dry at room temperature. Subsequently, they were imaged in air under ambient conditions, employing etched silicone probes with a tip radius of 5–10 nm and spring constant in the range of 20–100 N/m, oscillated at its fundamental resonant frequency (200–400 KHz).

Table 1
Formulation parameters for different nanosphere batches: polymer(s) used, initial RA-loading, and percentage of co-surfactant (n-butanol) in the organic phase.

Batch name	Weight ratio of polymer(s) used (w:w:w)			Co-surfactant (%, v/v)	Initial DNA-loading (μg per mg of polymer)	Initial RA-loading (μg per mg of polymer)
	PCL	Multiblock	PLA	(n-Butanol)		
Re2PLA	0	0	1	0	5	20
Re2PCL	1	0	0	0	5	20
BuRe2PCL	1	0	0	16.6	5	20
MuRe2PCL	2	1	0	0	5	20
Re3PCL	1	0	0	0	5	30
PLA	0	0	1	0	5	0

2.7. Surface area and porosity of nanospheres

Total surface area and porosity of the freeze-dried nanospheres were determined by the nitrogen isotherm adsorption and desorption technique in an automated gas sorption system (Autosorb-1™, Quantachrome Corporation, Boynton Beach, FL, USA). In brief, 100–150 mg of nanospheres were placed in glass sample holders and outgassed at room temperature (20 °C) for 3 h before analysis. Sample and reference tubes were then immersed in liquid nitrogen at −196 °C, and sorption isotherms were obtained from the nitrogen volume (cm^3/g) adsorbed onto the surface of the nanoparticles as a function of relative pressure. Surface area was calculated by the Brunauer–Emmett–Teller (BET) method (Brunauer et al., 1938), with five adsorption points in the P/P_0 range of 0.05–0.3.

2.8. Determination of DNA and RA EE in nanospheres

Ten milligrams of lyophilized nanospheres were weighed in sterile vials and re-dispersed in 3 mL PBS, pH 7.4. The dispersed nanospheres were then lysed with 2 mL chloroform, and extraction was facilitated by rotating the vials end-over-end in a rotating plate for 6 h at ambient temperature. The samples were centrifuged at 14,000 rpm for 5 min, and 500 μL of the aqueous supernatant were drawn off with micro-tipped pipettes. DNA and the extracted portion of RA in the aqueous layer were simultaneously quantified by the ^{2}D method. The remaining upper aqueous layer was pipetted out, and 0.5 mL of the organic phase was mixed with 4 mL methanol to precipitate the polymer. The obtained solution was then centrifuged at 14,000 rpm for 5 min, and 1 mL of the supernatant was brought to 10 mL with methanol. RA was measured at 352 nm, and its concentration was calculated with reference to a standard calibration curve. RA fractions in aqueous and organic phases were summed up to obtain total drug content of the tested sample. The validity of the described technique for the determination of extracted ingredients from loaded nanospheres was confirmed by the standard addition method for both RA and DNA, using empty nanospheres.

Particle size of the fresh nanospheres was estimated by photon electron spectroscopy (Nanosizer N4 Plus, Coulter Electronics, Hialeah, FL, USA), with a 62.5° angle of measurement and a run time of 300 s. The mean of at least three readings was calculated.

2.9. Release studies

Five milligrams of nanospheres were accurately weighed and transferred to glass vials with tight caps. The nanospheres were dispersed in 10 mL of sterile PBS, and argon gas was purged from the release medium, with each vial being hermetically sealed and protected from light. The samples were agitated at 75 rpm in an orbital shaking incubator where the temperature was adjusted to 37 °C, and aliquots were taken according to prescheduled time intervals. The absorbance signal of RA was detectable in the release medium which permitted its spectrophotometric quantification by the second derivative technique. However, DNA had to be complexed with ethidium bromide prior to spectrofluorometric determination (Rengarajan et al., 2002).

2.10. Assessment of the anti-angiogenic effect

An established tissue culture model of rat aortic rings was adapted for this purpose (Girardot et al., 2004). First, 24-well culture plates were pre-coated with collagen gel which had been prepared by quickly mixing rat tail collagen solution (3 mg/mL), Dulbecco's Modified Eagle Medium (DMEM) supplemented with 7% fetal calf serum and glutamine, and 1 mL 0.1N sodium hydroxide (6:7.5:1) at 4 °C. Gelation was allowed for 1 h at 37 °C after coating each well with 0.5 mL of the mixture. Later, 1-mm thick rings of cleaned aortae were prepared in sterile Hanks balanced salt solution (HBSS), and then carefully placed in the collagen pre-coated wells. Twenty microliters of the tested preparation (either free RA solution or nanosphere dispersion in 0.25% (w/v) Tween 80 in HBSS) were pipetted on the center of each aortic ring. Being a common vehicle for all tested samples, a blank solution of Tween 80 in HBSS was applied at 20 μL per well to obtain positive control wells, whereas negative control wells were spared from any treatment. The 24-well plates were incubated at 37 °C for 20 min, followed by the application of a second layer of collagen mixture on each well. After gelation, an enriched medium consisting of supplemented DMEM, endothelial cell growth supplement (15 mg/mL), epidermal growth factor (10 ng/mL) and insulin (5 μg/mL) was added to the wells, and the culture was incubated at 37 °C in 5% carbon dioxide atmosphere.

The embedded aortic rings were observed every second day under an inverted microscope at 40×. The growth of new tubules and their ramifications were quantified on images captured from the wells on the 7th and 14th days of culture by a digital camera (Canon PowerShot A95), after photo binarization to black/white with Paint Shop Pro® software. Vascular density was then analyzed by image analysis software (Optimas 7®) and expressed as the percentage of blackened tubules relative to whitened background.

3. Results and discussion

3.1. Second derivative spectrophotometric analysis

In the present study, significant interference was observed between the absorption spectra of DNA and RA, rendering their direct quantification inaccurate. Derivative techniques were applied for spectrophotometric data treatment, as a powerful and simple tool, to enhance the accuracy of both qualitative and quantitative analyses of the pharmaceutical mixtures. Such an approach is particularly helpful when the signal is weak or when different signals interfere conjointly (Mabrouk et al., 2003).

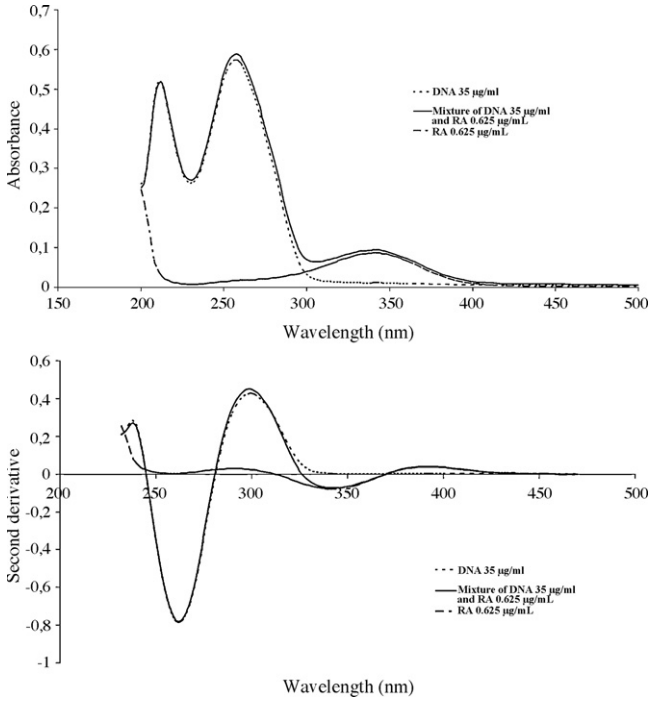

Fig. 1. (A) Absorbance spectra of standard solutions of DNA, RA, and their mixture in PBS, pH 7.4. (B) Second derivative spectra of DNA, RA, and their mixture in PBS, pH 7.4.

The experiments achieved showed that second derivative (^{2}D) absorbance was useful for the elimination of most interference. Hence, the spectra of the prepared mixtures were recorded, and the corresponding ^{2}D data were computed and plotted. With each mixture, the amplitude of the valley at 262 nm was measured for DNA determination in the presence of RA, whereas peak to valley values at 342 and 392 nm, respectively, were summed for the quantification of RA in the presence of DNA.

The absorption spectra of DNA and RA single-component solutions at given concentrations plus those of their corresponding binary mixture are depicted in Fig. 1A, where mutual influence on the absorption peaks of each ingredient can be noticed in the mixture spectrum in comparison to the corresponding peaks in spectra of single-component solutions. ^{2}D plots of the absorption spectra (Fig. 1B) show that such mutual interference was abolished as the binary mixture ^{2}D curve fitted well with each of the single-component curves, at those spots previously assigned for individual ingredients. Calibration curves with ^{2}D for both agents were constructed and validated for analytical data and regression characteristics (Table 2). Finally, the obtained recovery values from the synthetic mixtures ranged from 98.0 to 101.2% (mean ± S.D. = 99.5 ± 1.1) for RA(I), and from 98.5 to 101.8% (mean ± S.D. = 99.5 ± 0.9) for DNA(II).

3.2. DSC analysis

Fig. 2A presents DSC thermograms of RA and blank PCL nanospheres, in addition to drug-loaded PCL nanospheres Re2PCL, BuRe2PCL, and Re3PCL. Thermal tracing of RA exhibited a well-defined, narrow endothermic peak at 185.13 °C corresponding to fusion. Similarly, blank PCL nanosphere thermograms were depicted as a fairly deep symmetric peak with T_m at 54.6 °C corresponding to melting of the polymer. This finding confirms the semi-crystalline nature of PCL (Jeong et al., 2003). Drug-loaded PCL nanospheres containing 2% RA did not manifest any thermal

Table 2
Data analysis and regression characteristics of RA(I) and DNA(II) according to the ^{2}D method.

Parameters	Compounds	
	(I)	(II)
Linearity range (μg ml^{-1})	0.125–1.25	5–50
Detection limit (μg ml^{-1})	0.015106	3.251×10^{-4}
Quantification limit	0.050305	1.0827×10^{-3}
Regression equation (y)[a], slope (b)	0.1862	0.0224
S.D. of the slope	1.630×10^{-3}	4.233×10^{-6}
Variance of the slope	2.658×10^{-6}	1.792×10^{-11}
Confidence limit of the slope (95% confidence limit)	$\pm 3.032 \times 10^{-3}$	$\pm 7.663 \times 10^{-6}$
Intercept[a] (a)	0.0008	0.0038
S.D. of the intercept	1.264×10^{-3}	1.253×10^{-4}
Variance of the intercept	1.599×10^{-3}	1.569×10^{-8}
Confidence limit of the intercept (95% confidence limit)	$\pm 2.352 \times 10^{-3}$	$\pm 2.267 \times 10^{-4}$
Correlation coefficient (r)	0.9996	0.9999
Relative standard deviation (%)[b]	2.076%	1.084%

[a] $y = a + bc$, where c is the concentration in μg ml^{-1} and y is the 2D amplitude for valley to peak at 342 and 392 nm, respectively for I, and at 262 nm for II.
[b] For 10 replicate samples of each pure compound.

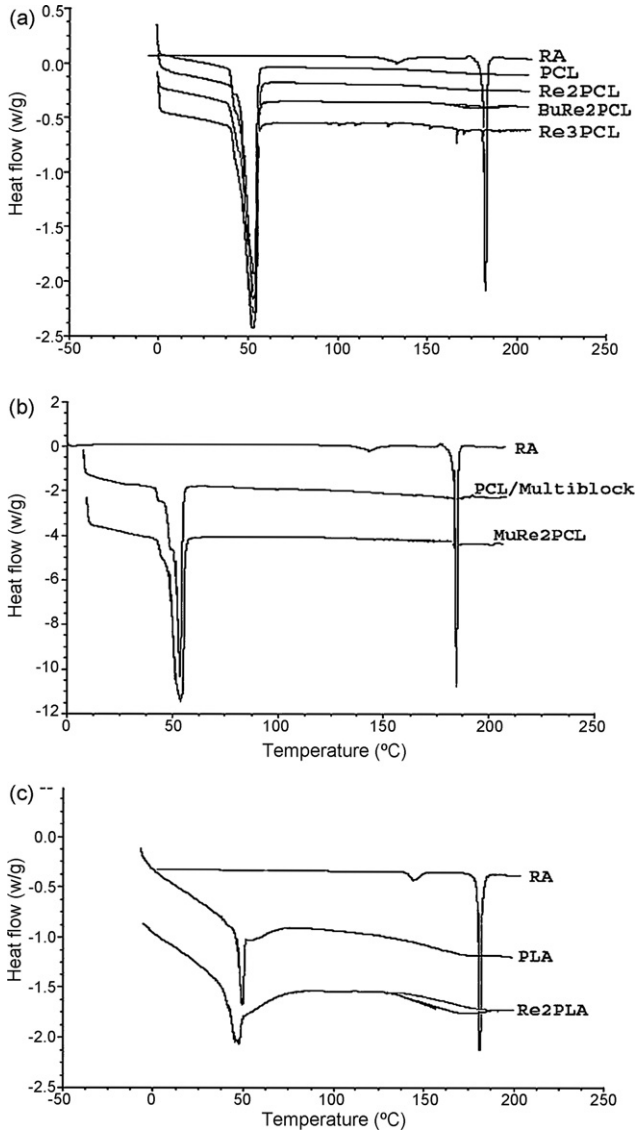

Fig. 2. (A–C) DSC thermograms of pure RA and different nanosphere batches.

transition corresponding to the loaded drug, in the 150–250 °C temperature range, possibly accounting for molecular dispersion of the drug as a solid solution in the polymer matrix after production (Dubernet, 1987). Regarding PCL nanospheres incorporating 3% of RA, i.e. the Re3PCL batch, no fusion event was observed for the drug, although some deviations from baseline could be seen in the drug-melting range. This could be explained by the degradation of crystalline RA traces that may be deposited in the polymeric matrix during solvent removal and/or the lyophilization procedure. However, nanospheres prepared with n-butanol as co-surfactant for the primary w/o emulsion (BuRe2PCL batch) showed limited re-crystallization of RA, as deduced from the observed shallow peak related to drug fusion (ΔH = 2.04 J/g). Such re-crystallization could be attributed to the drug fraction extracted from the preformed nanospheres by the partially water-miscible n-butanol in the course of the secondary emulsification procedure. A part of the escaped drug could subsequently be readsorbed to the particle surface after diffusion of the organic co-solvent in the external aqueous phase. On the other hand, demarcation of the RA-melting event was quite difficult to detect in thermal traces corresponding to MuRe2PCL nanospheres (Fig. 2B).

In Fig. 2C, thermograms of the nanospheres made of pure PLA polymer exhibited relatively broad and distorted thermal transition (T_g at 58.1 °C), confirming the amorphous nature of PLA. From DSC tracings of the corresponding Re2PLA nanospheres, thermal transition with T_{max} at 173.9 °C and ΔH of 4.06 J/g was observed. This endotherm can be easily attributed to the melting of RA crystalloids that persists in the formulation in spite of the filtration/primary centrifugation pretreatment procedures aiming to remove drug crystals precipitated during the preparation of this batch. Nevertheless, the drug endothermic peak was flattened and less symmetric compared to the pure RA endotherm, perhaps due to the partial loss of crystallinity and the high state of subdivision of its deposit in PLA nanospheres.

3.3. Morphology and particle size of nanospheres

The AFM technique is widely applied as a characterization tool for particulate drug carriers, being able to provide three-dimensional images of surface topography at nanometric resolution (Garg and Kokkoli, 2005). Fig. 3A and B illustrate the drug-loaded nanospheres made from PCL, namely, Re2PCL and BuRe2PCL. Both types of nanospheres were spherical, more or less discrete, with apparently smooth surfaces, and no surface irregularities. Images of the MuRe2PCL batch are exhibited in Fig. 3C, where significant deformation and flattening can be easily noticed. Such findings may be explained by incorporation of the multiblock copolymer $(PLA\text{-}PEG\text{-}PLA)_n$ in the polymer blend of this

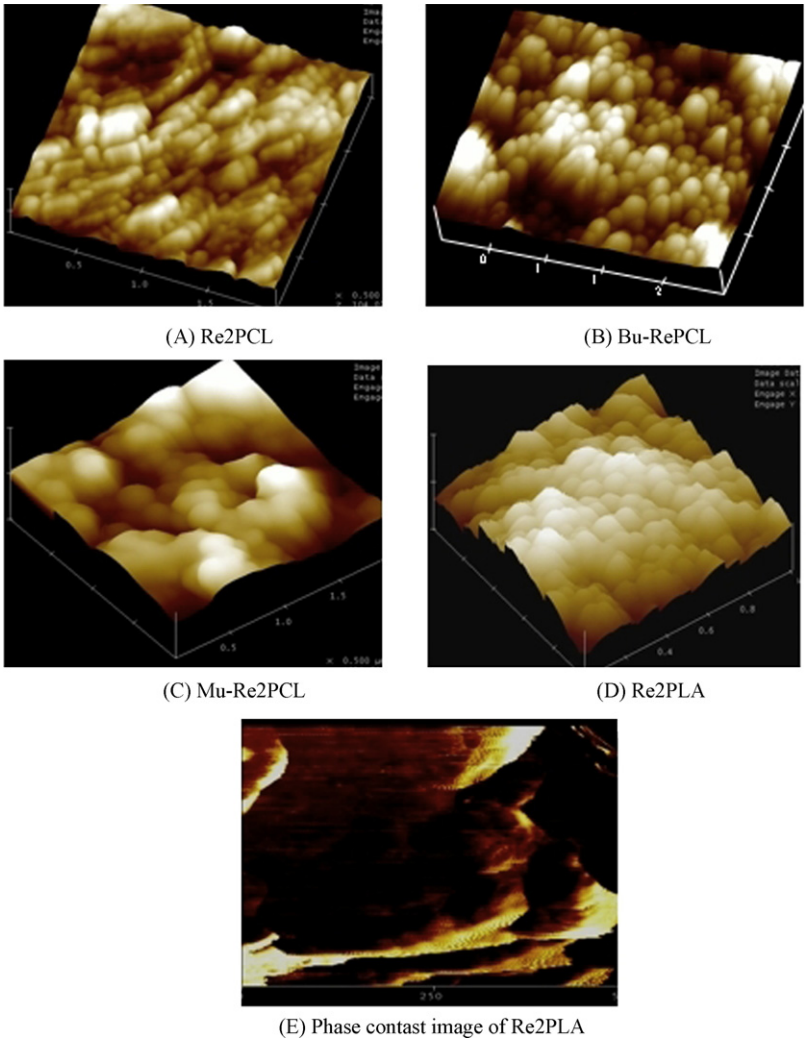

Fig. 3. (A–E) AFM images of nanospheres. The scale for all images is 2 μm except for image (B), where it is 10 μm.

Table 3
Percentage encapsulation efficiency (% EE), loading of RA and DNA, and particle size of prepared nanosphere batches (mean ± S.D. for $n = 3$).

Batch name	DNA % EE (mean ± S.D.)	DNA-loading (μg per mg polymer)	RA % EE (mean ± S.D.)	RA-loading (μg per mg polymer)	Particle diameter (nm)
Re2PLA	38.2 ± 2.2	1.91	66.9 ± 1.4	13.37	302.9 ± 10.4
Re2PCL	16.9 ± 1.1	0.85	77.0 ± 1.8	15.40	243.8 ± 21.5
BuRe2PCL	37.0 ± 3.7	1.85	56.1 ± 2.3	11.21	238.7 ± 28.9
MuRe2PCL	55.1 ± 4.4	2.76	63.3 ± 1.7	12.65	228.4 ± 26.0
Re3PCL	17.2 ± 1.4	0.86	60.1 ± 2.2	18.04	260.5 ± 32.2

batch. These copolymers are well-known to result in poorly formed nano/microspheres due to the high hydration characteristics of the PEG moiety and its plasticizing effect (Huang and Chung, 2001). Consequently, this will have an obvious impact on the final product, resulting in softening of the nanospheres and their deformation during sample preparation for AFM imaging. On the other hand, Re2PLA nanospheres manifested needle-like irregularities adhering on their surface (Fig. 3D). Indeed, the tapping mode yielding phase images of these nanospheres confirmed the presence of shiny dots (corresponding to a harder region) on a darker background (softer region) of the polymeric matrix (Fig. 3E). In light of the DSC data discussed earlier, this observation may be explained by the persistence of RA crystalloids on the surface of Re2PLA nanospheres.

Finally, AFM topographic measurement of particle diameter of the visualized nanospheres revealed average diameter values of 217.4, 232.2, 272.0, and 285.1 nm for Re2PCL, BuRe2PCL, MuRe2PCL, and Re2PLA nanospheres, respectively. These results are in good accordance with the particle size determination data provided by the photocorrelation spectroscopy technique (Table 3).

3.4. Porosity and surface area

Small pores in polymeric nanoparticles can affect matrix hydration, drug diffusion into the release medium, and polymer erosion (Petrov et al., 2006). In this respect, analysis of nitrogen adsorption isotherms represents a practical tool for the assessment of a wide range of pore sizes, including the complete range of micro- (0.32–2 nm) and mesopores (2–50 nm). It has been demonstrated recently that an appropriate data analysis method to process adsorption/desorption isotherms will provide high resolution for adequate characterization of nanosphere microporosity (Sant et al., 2008). In the present study, micropore data analysis was performed according to the Dubinin–Radushevich method (Dubinin, 1989), where average values of pore volume, pore surface area and pore width of the prepared batches were calculated. In addition, multipoint BET surface area values were determined, and all data presented in Table 4. It was quite evident that pore width values mainly reflected mesopores rather than micropores as these values appeared to be barely affected by the microporosity variations between different nanosphere batches. Alternatively, the values of the other parameters seemed to be directly related to porosity of the nanosphere matrix.

The microemulsion approach (Span 80/n-butanol) for the preparation of primary w/o emulsions in the course of PCL nanosphere manufacturing has remarkably reduced the porosity of the resulting product (BuRe2PCL) in comparison to Re2PCL, as reflected by lower porosity values (Table 4). This could be attributed to the enhanced stability and fineness of the primary w/o emulsions acquired during the preparation of nanospheres (Hammady et al., 2006). Nevertheless, a more pronounced reduction of porosity could be observed in nanospheres made of PCL-multiblock polymer blend. Incorporation of the PEGylated polymer in PCL nanospheres significantly altered the microstructure of the final product. Relatively short PEG chains seemed to be able to fill the voids between longer polyester chains, and this would therefore result in reduced porosity of the nanosphere matrix (Rizkalla et al., 2006; Sant et al., 2008). On the other hand, raising initial RA-loading in the PCL nanospheres had little effect on product porosity.

Re2PLA nanospheres manifested apparently high porosity, as depicted by elevated porosity values relative to those reported for other batches. In light of AFM imaging and the DSC data, such results may be explained by the presence of crystals within the matrix of Re2PLA nanospheres, due to RA deposition. The intermingling of polymer chains with RA crystals is likely to result in a highly heterogeneous matrix, which, in turn, may account for elevated matrix porosity. Oppositely, DNA-loaded PLA nanospheres (with no loaded RA) showed reduced porosity relative to Re2PLA, yet still much higher porosity than Re2PCL nanospheres.

3.5. DNA and RA EE in nanospheres

Data on % EE, drug loading, and particle size of the nanospheres are presented in Table 3. For the Re2PLA batch, initial RA-loading of 20 μg per mg polymer evoked obvious drug crystallization in the external aqueous phase once w/o/w emulsion was obtained during the preparation procedure. Before the assessment procedure, it was necessary to get rid of the precipitated RA fraction since it does not contribute to the actual drug content of nanospheres. Hence, after removal of non-incorporated RA, the % EE of the drug in Re2PLA nanospheres was found to be 66.9% compared to 77.0% for the Re2PCL batch that showed no visible drug precipitation. This phenomenon could be explained by the more hydrophobic character of PCL, which renders it more convenient to incorporate larger amounts of the highly lipophilic RA in the form of molecular dispersion, as discussed earlier. Nevertheless, the percentage of loaded RA did not exceed ~60.1% when initial drug loading was raised to 30 μg per mg polymer.

Alternatively, the capacity of PCL to encapsulate DNA is limited by its high hydrophobic character. We speculated that the poly-

Table 4
Porosity and surface area parameters of RA-DNA-loaded nanospheres prepared by the double emulsion method (mean ± S.D. for $n = 3$).

Formula	Average pore width (nm)	Micropore volume (cc/g)	Micropore surface area (m^2/g)	BET surface area (m^2/g)
Re2PCL	4.504 ± 0.242	$8.57 \times 10^{-4} \pm 0.43 \times 10^{-4}$	2.41 ± 0.21	8.01 ± 0.33
BuRe2PCL	4.203 ± 0.174	$3.64 \times 10^{-4} \pm 0.74 \times 10^{-4}$	1.02 ± 0.21	5.00 ± 0.85
MuRe2PCL	3.912 ± 0.205	$1.31 \times 10^{-4} \pm 0.24 \times 10^{-4}$	0.37 ± 0.07	3.23 ± 1.17
Re3PCL	4.380 ± 0.039	$5.88 \times 10^{-4} \pm 0.57 \times 10^{-4}$	1.65 ± 0.16	7.19 ± 0.92
Re2PLA	4.765 ± 0.183	$5.92 \times 10^{-3} \pm 0.67 \times 10^{-3}$	16.64 ± 1.89	26.62 ± 4.42
PLA	4.085 ± 0.041	$4.36 \times 10^{-3} \pm 0.73 \times 10^{-3}$	12.33 ± 2.03	18.96 ± 5.50

mer's hydrophobic domains did not help in stabilizing the primary emulsion in the course of nanosphere preparation by the double emulsion technique, even in the presence of surfactant in the organic phase. This has been reported to limit the encapsulation of hydrophilic ingredients in nano/microspheres, even with less hydrophobic polymers (Ruan et al., 2004).

To find a compromise in addressing this problem, we tried two different approaches. The first one was the microemulsion technique associating a co-solvent (n-butanol) with the surfactant incorporated in the organic phase of the primary emulsion, to enhance its stability and, hence, to increase the EE of hydrophilic macromolecules such as proteins and DNA (Hammady et al., 2006). Secondly, we tried to reduce the hydrophobic character of PCL by confecting a hybrid nanosphere matrix consisting of PCL and the more hydrophilic multiblock $(PLA\text{-}PEG\text{-}PLA)_n$ copolymer. The hydrophilic PEG moiety in the copolymer seemed not only to enhance the stability of the primary emulsion, but is thought to also improve the affinity of the matrix for hydrophilic DNA by promoting its hydration (Bouillot et al., 1999; Pistel et al., 2001). This may explain the more prominent positive effect on DNA-loading in the latter case. Nevertheless, such attempts induced a more or less negative effect on RA-loading in nanospheres since a more hydrophilic matrix is less favourable for the retention of the highly lipophilic RA. Therefore, a wise selection of polymer proportions is crucial to ensure an acceptable compromise of % EE of both ingredients. Based on preliminary trials, a ratio of 1–2 (w:w) appears to be suitable to achieve this goal. Alternatively, a partially water miscible solvent as co-surfactant may facilitate the extraction and, hence, partial loss of the drug into the external aqueous phase during the secondary emulsification and subsequent solidification step, as discussed earlier.

It can be easily observed that nanosphere-loading capacity towards RA is directly related to the size of the hydrophobic domains in their matrix. Multiblock copolymer is more hydrophilic than PLA which itself is more hydrophilic than PCL. One should notice that the hydrophilic domains of the multiblock copolymer represents one-third of the MuRe2PCL formula matrix, whereas the other two-thirds are formed by the highly hydrophobic PCL domains. This renders the MuRe2PCL matrix less favorable for RA incorporation compared to Re2PCL, formed entirely by PCL domains. Similarly, the PLA matrix, being intermediate in its hydrophobic character between PCL and PEGylated copolymer, shows only a slightly higher loading capacity for RA than the $PCL\text{–}(PLA\text{-}PEG\text{-}PLA)_n$ polymeric blend (% EEs are 66.9 and 63.3%, respectively). However, we consider that a significant portion of RA in Re2PLA nanospheres is retained as drug crystalloids rather than molecular dispersion, as evidenced by DSC analysis.

3.6. Release studies

As reported in earlier work, it is not likely that polymer erosion significantly contributes to the release process under the conditions of our study (Sinha et al., 2004). The release patterns revealed biphasic behaviour in general, where variable initial burst effects were manifested, followed by slower release of the loaded drug. The burst effect is mainly attributed to the desorption of unwashed drug at the surface of polymeric carriers. This phenomenon is more prominent in the case of nanospheres than in microspheres due to the larger surface area exposed to the medium (Nkansah et al., 2008). In the second phase, release was mainly controlled by diffusion through channels connected to surface-forming pores.

Fig. 4 shows the *in vitro* release of RA from different batches of nanospheres, where a considerable burst effect was exhibited by the Re2PLA batch and, to a lesser extent, by the BuRe2PCL preparation (49.1 and 40.0% after 24 h, respectively). Such an effect may be easily attributed to dissolution of the loosely bound or embedded drug on the nanosphere surface (Chen et al., 2005). Indeed, the presence of RA crystalloids was evident in the two-mentioned batches by DSC measurements; moreover, it was thought to be emphasized by the AFM imaging of Re2PCL nanospheres. On the other hand, steady drug release was exhibited by the Re2PCL batch with little burst effect. Based on the DSC data, we can assume that the highly hydrophobic character of PCL promotes the retention of finely dispersed lipophilic RA in the polymeric matrix. The reduced microporosity of the MuRe2PCL batch may account for the relatively slow release of RA from these nanospheres, exhibiting a remarkably smooth pattern of initial release.

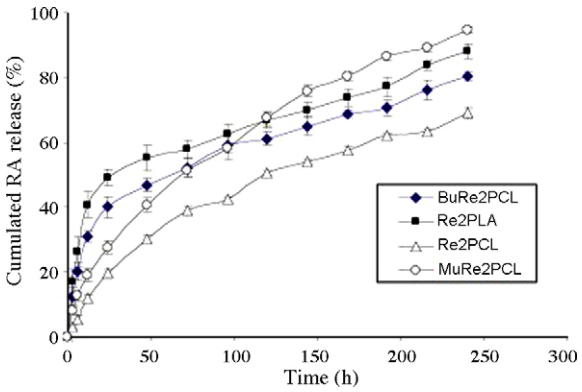

Fig. 4. *In vitro* release of RA from nanospheres in PBS, pH 7.4, at 37 °C ($n = 3$, ±S.D.).

Concerning DNA release from the tested nanospheres (Fig. 5), the highest burst effect was seen with Re2PLA (~40.6% over a 24-h period) which could be explained by the dissolution of unwashed DNA molecules on the external surface of the particles or entrapped in pores of their outer skin layer. On the other hand, a less prominent burst effect was observed with PCL nanospheres, namely, 22.8 and 33.4% after 24 h for BuRe2PCL and Re2PCL, respectively. The amphiphilic nature of PLA may allow the retention of a portion of initially loaded DNA at the particle surface, even after the washing procedure. Moreover, it has been reported that microencapsulated macromolecules migrate to and concentrate near or on the nanosphere surface when vacuum-dried (Pistel and Kissel, 2000). This assumption may clarify the role of microporosity in the burst effect as well, since elevated porosity would facilitate such superficial translocation.

After the initial burst, the DNA release profiles displayed a more or less slow pattern until the end of the study. In an attempt to elucidate the relationship between the DNA release rate and nanosphere

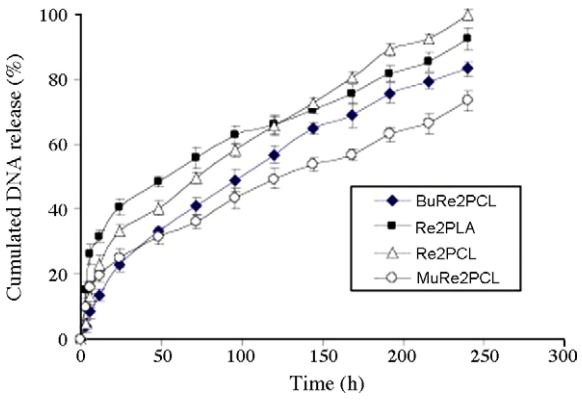

Fig. 5. *In vitro* release of DNA from nanospheres in PBS, pH 7.4, at 37 °C ($n = 3$, ±S.D.).

microporosity, DNA release rate constants for Re2PCl, BuRe2PCL and MuRe2PCl nanosphere batches were expressed by calculating the linear regression coefficients for their release curves in the region between 24 and 240 h (to avoid the influence of the burst effect). Then, the obtained data were correlated with the corresponding values of micropore volume taken as a microporosity parameter. The r^2 value was found to be 0.85, demonstrating a fair correlation between the microporosity data (Table 4) and DNA release rates from different batches. Therefore, it can be deduced that the higher the microporosity, the easier was matrix hydration and the diffusion of DNA molecules through the micropores to the aqueous medium (Sant et al., 2008). In addition, it should be noted that the hydrophilic nature of the multiblock copolymer may further slow DNA release from MuRe2PCL nanospheres through high affinity of the PEG moiety for the hydrophilic macromolecule and/or formation of a reservoir phase of the PEG outer shell that controls its diffusion (Pistel et al., 2001; Gref et al., 2001).

It could be noticed that the release curves showed no tendency to level out while approaching towards the end of the experiment, as is supposed to take place. Such a phenomenon was seen before in other publications (Panoyan et al., 2003). In fact, this is more likely to happen when amphiphilic macromolecules, such as multiblock copolymers and/or lipophilic surfactants (Span 80 in the present case), are incorporated in the nanosphere matrix. Such macromolecules tend to form microdomains within the polymeric matrix that act as secondary microreservoirs of the encapsulated ingredient(s) (Gupte et al., 1991; Kikkinides et al., 1998). Drug diffusion from such microdomains may follow a different pattern than that of the drug portion dispersed homogeneously in the rest of the polymeric matrix. Drug molecules entrapped in microdomains leach out to diffuse through the bulk polymeric matrix before reaching the nanosphere interface with the aqueous release medium. According to Kikkinides et al., such internal diffusion is mainly responsible for the dispersive behaviour of the flux following the plateau region, which, in turn, leads to unexpected variations in the release rate as drug depletion from the nanospheres proceeds (Kikkinides et al., 1998).

3.7. Inhibition of angiogenesis

Being an angiosuppressive molecule, the biological activity of microencapsulated RA was evaluated in this study using the rat aorta model. Re2PLC and Re2PLA batches were prepared with no loaded DNA, to test the anti-angiogenic effect of microencapsulated RA versus free RA. *T*-test served to compare the two data sets. Figs. 6 and 7 show representative samples of rat aortic tissue cultured for 7 and 14 days, respectively, for the assessment of control and treatment parameters. The vascular density of all

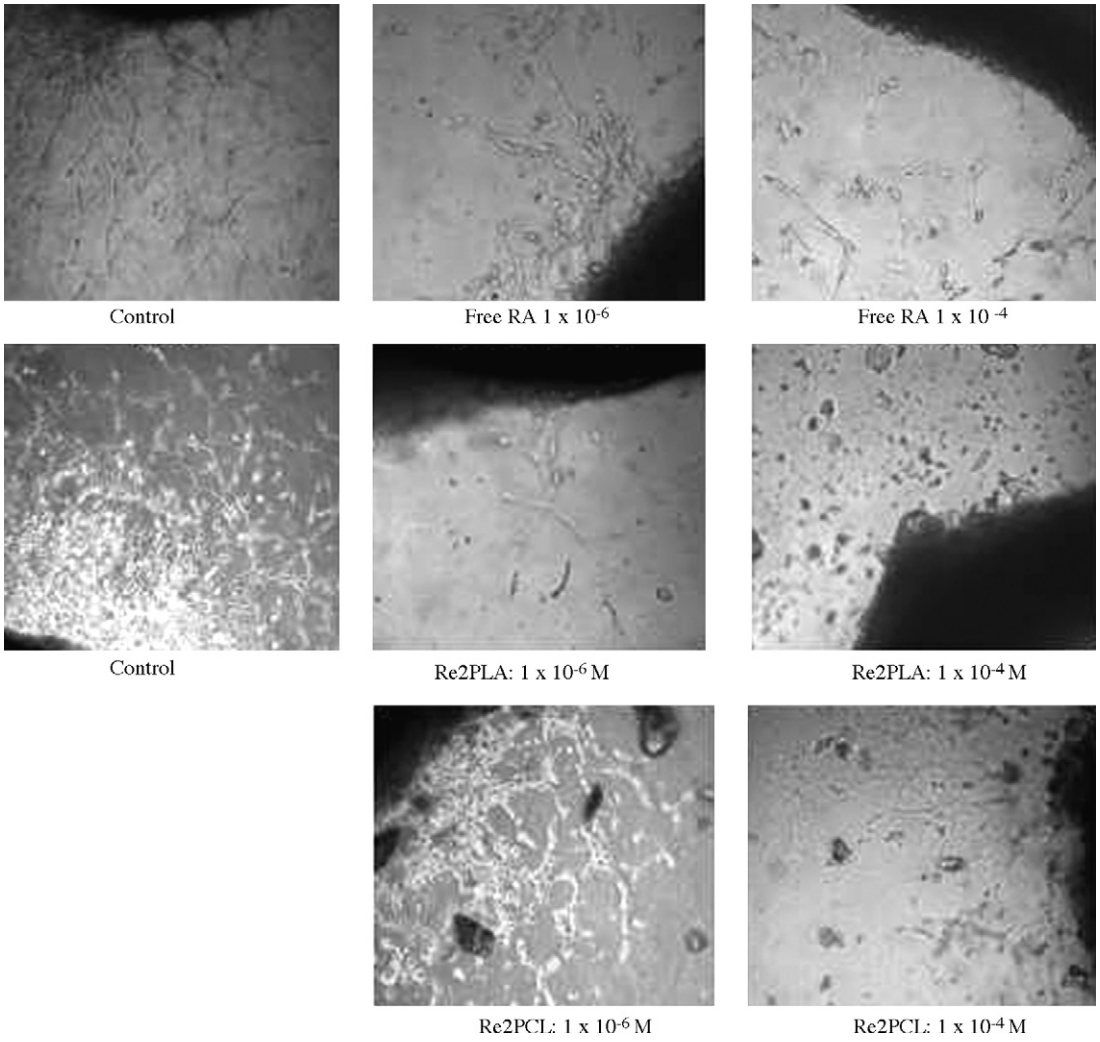

Fig. 6. Micrograph of growing tubules (40×) across the collagen matrix. A part of the aortic ring is observed in the corner of each picture. Experiments were performed with free and encapsulated RA versus control after 7 days.

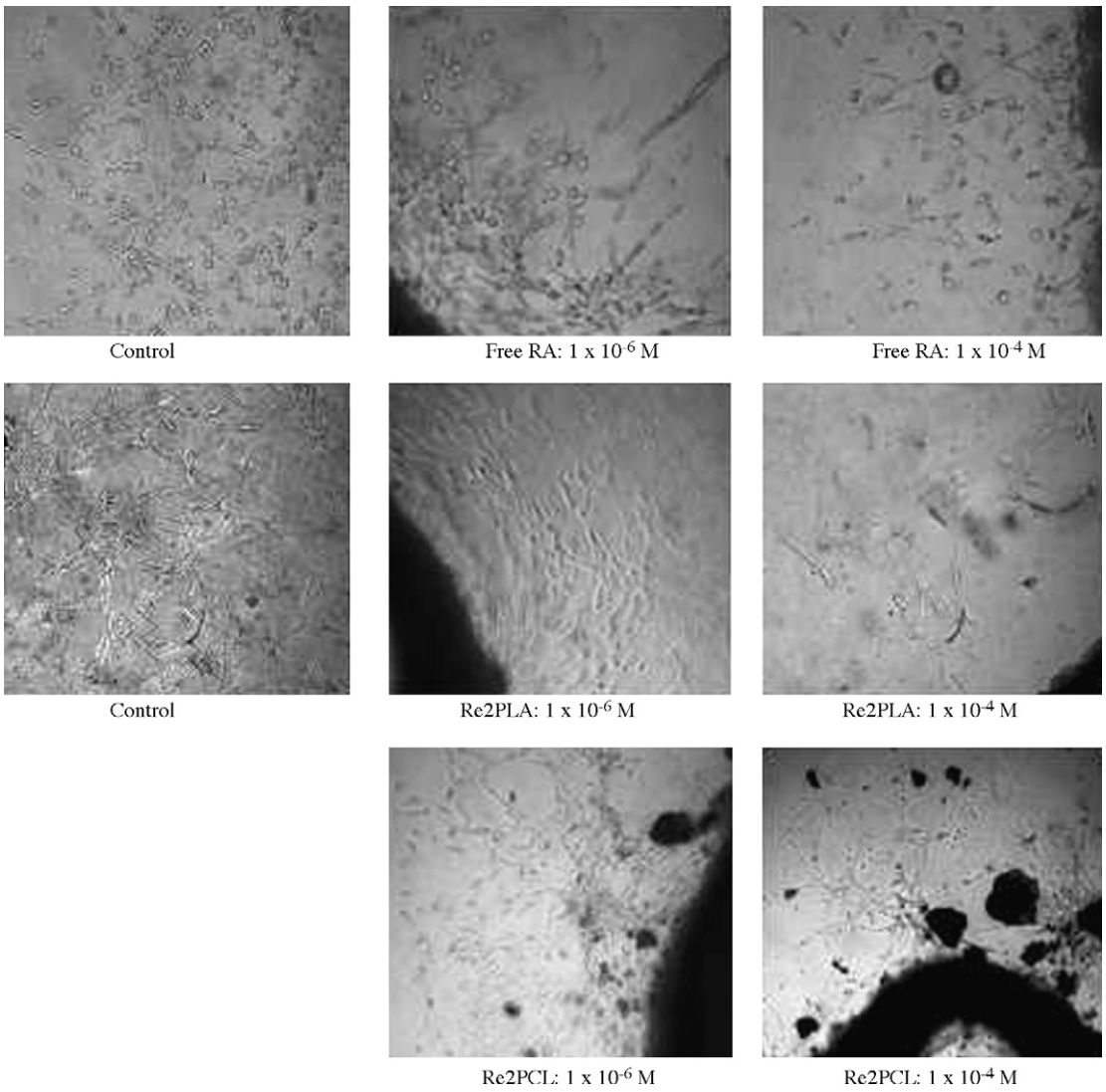

Fig. 7. Micrograph of growing tubules (40×) across the collagen matrix. A part of the aortic ring is observed in the corner of each picture. Experiments were performed with free and encapsulated RA versus control after 14 days.

treated cultures was obviously less than that of the positive control series, whether RA was free or loaded in nanospheres. It is noteworthy that empty nanospheres made from PLA and PCL were also tested, and the resulting vascular densities were comparable to data obtained from negative and positive control wells (data not shown). This lends support to the biocompatibility of these polymers, as reported in the literature. For comparative purposes, % inhibition was calculated with reference to the average of corresponding control values, and all data were tabulated in Fig. 8. By the 7th day, it was evident that the most powerful inhibition was induced by Re2PLA nanospheres for both drug concentrations, but especially at 1×10^{-4} M of RA (significant at $P = 0.01$). On the other hand, free RA showed a slightly greater inhibitory effect than Re2PCL at 1×10^{-6} M of RA ($P = 0.24$); however, it was the inverse for the 1×10^{-4} M series ($P = 0.32$).

After 14 days, the Re2PLA batch remained superior in terms of its anti-angiogenic action. One explanation could be the considerable burst effect of the anti-angiogenic drug, as observed from its release profile, followed by slower release of the remaining encapsulated cargo. This seems to ensure a highly potent loading dose, followed by some steady supply that supports its initial inhibitory action throughout the study period. Regarding the Re2PCL batch,

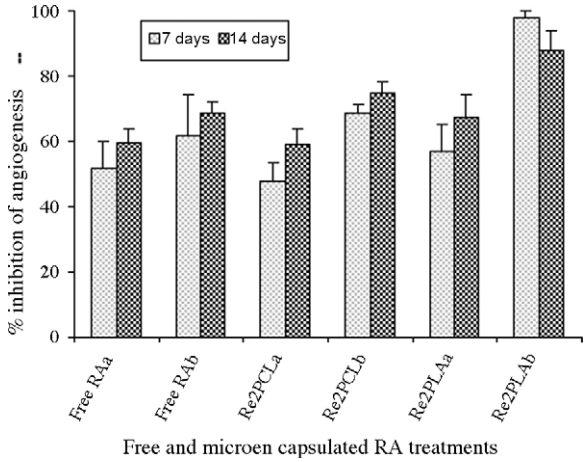

Fig. 8. Inhibition of angiogenesis in rat aortic ring tissue culture in response to free or loaded RA after 7 and 14 days.

its inhibitory effect was very close to that attributed to free RA at 1×10^{-6} M (59.1 and 59.6%, respectively), whereas PCL nanospheres continued to be more potent at the higher concentration ($P = 0.12$). In this context, a little burst effect and highly controlled drug release may explain the variability of the dose action induced by Re2PCL. It is likely that at higher concentrations, the nanospheres protected and released enough of the intact drug in the course of the study. These characteristics probably helped to surpass free RA at the higher concentration, since free RA is a highly unstable molecule (Ioele et al., 2005).

With reference to the aqueous release medium, we can presume that the mobility of the RA molecule may be reduced by elevated viscosity of the 3D collagen matrix. Nevertheless, it was found that regular collagen did not significantly hinder the diffusion of most drug molecules because its large effective pore size reached tens of nanometers (Wallace and Rosenblatt, 2003). Hence, we thought that a 7-day period from the start of culture was more than enough for RA molecules (M_w 300) to diffuse uniformly throughout the collagen-based culture medium and to induce its angiosuppressive action observed above.

4. Conclusion

The concomitant encapsulation of a hydrophilic with a lipophilic macromolecule in polymeric nanospheres represents a challenge due to the difficult technical compromises needed to obtain the satisfactory encapsulation of both cargos. Moreover, RA is a difficult drug encapsulation model, even in solid lipid nanoparticles (Jenning and Golan, 2001). In this work, we have tried the association of PCL with PEGylated copolymer and the microemulsion technique for the co-encapsulation of selected models. In addition, PLA was used for comparison, being less hydrophobic and less crystalline than PCL. We conclude from the results that the polymer blend may offer a fairly acceptable compromise for our purpose although this does not exclude the microemulsion approach for other drug combinations. The quantification of RA and DNA with derivative spectrophotometry was successful for encapsulation assessment, whereas the DNA signal in the buffer medium was too weak to be reliable in release studies. Because of this inconvenience, we shifted to the classical spectrofluorometric method to quantify DNA. Nevertheless, the derivative technique was still valid for RA determination in our experiments. Thermal analysis, porosity measurement, and AFM imaging served to monitor the different preparations. DSC mainly revealed the dispersion state of RA in the polymer matrix which provided a better insight into its encapsulation pattern. On the other hand, reduced porosity may express enhanced stability of the primary emulsion, and these two interrelated aspects augmented DNA retention in the nanospheres. We can conclude that both the nature of the polymeric matrix and porosity play major roles in release behaviour. Reduced porosity contributes considerably to slowing the release of both RA and DNA. Nevertheless, the degree of RA crystallization was directly responsible for its early release pattern. Rat aorta tissue culture served as an *ex vivo* model for evaluation of the biological effect of both free and loaded RA. The data obtained were well correlated with the release pattern of the tested batches. The applicability of rat aorta tissue culture to test the activity of the microencapsulated anti-angiogenic agent has thus been established. Finally, we have to emphasize that our ultimate target is to substitute the calf thymus DNA model by a hydrophilic anti-angiogenic molecule, e.g. a protein or a DNA plasmid coding for a protein, concomitantly with a lipophilic anti-angiogenic drug. This work will be published soon in a separate paper as the large amount of data obtained cannot be presented in a single paper.

Acknowledgments

The authors thank the Natural Sciences and Engineering Research Council (NSERC) of Canada for financial support, and Groupe de Recherche Universitaire sur le Medicament (GRUM). The editorial work of Mr. Ovid Da Silva on this manuscript is acknowledged.

Appendix A. Supplementary data

Supplementary data associated with this article can be found, in the online version, at doi:10.1016/j.ijpharm.2008.10.034.

References

Bakris, G.L., 2008. Combined therapy with a calcium channel blocker and an angiotensin II type 1 receptor blocker. J. Clin. Hypertens. (Greenwich) 10, 27–32.
Blanco, M.D., Alonso, M.J., 1997. Development and characterization of protein-loaded poly(DL-lactide-co-glycolide) nanospheres. Eur. J. Pharm. Biopharm. 43, 287–294.
Bouillot, P., Babak, V., Dellacherie, E., 1999. Novel bioresorbable and bioeliminable surfactants for microsphere preparation. Pharm. Res. 16, 148–154.
Brigger, I., Dubernet, C., Couvreur, P., 2002. Nanoparticles in cancer therapy and diagnosis. Adv. Drug Deliv. Rev. 54, 631–651.
Brunauer, S., Emmett, P.H., Teller, E., 1938. Adsorption of gases in multimolecular layers. J. Am. Chem. Soc. 60, 309–319.
Chansri, N., Kawakami, S., Yokoyama, M., Yamamoto, T., Charoensit, P., Hashida, M., 2008. Anti-tumor effect of all-trans retinoic acid loaded polymeric micelles in solid tumor bearing mice. Pharm. Res. 25, 428–434.
Chen, X., Ooi, C.P., Lye, W.S., Lim, T.H., 2005. Sustained release of ganciclovir from poly(lactide-co-glycolide) microspheres. J. Microencapsul. 22, 621–631.
Choi, Y., Kim, S.Y., Park, K., Yang, J., Cho, K.J., Kwon, H.J., Byun, Y., 2006. Chemopreventive efficacy of all-trans-retinoic acid in biodegradable microspheres against epithelial cancers: results in a 4-nitroquinoline 1-oxide-induced oral carcinogenesis model. Int. J. Pharm. 320, 45–52.
Degim, I.T., Celebi, N., 2007. Controlled delivery of peptides and proteins. Curr. Pharm. Des. 13, 99–117.
Dong, W., Bodmeier, R., 2006. Encapsulation of lipophilic drugs within enteric microparticles by a novel coacervation method. Int. J. Pharm. 326, 128–138.
Dubernet, C., 1987. Thermoanalysis of microspheres. Thermochim. Acta 248, 69–76.
Dubinin, M.M., 1989. Fundamentals of the theory of adsorption in micropores of carbon adsorbents: characteristics of their adsorption properties and microporous structures. Carbon 27, 457–467.
El-Gindy, A., Ashour, A., Abdel-Fattah, L., Shabana, M.M., 2001. Spectrophotometric determination of benazepril hydrochloride and hydrochlorothiazide in binary mixture using second derivative, second derivative of the ratio spectra and chemometric methods. J. Pharm. Biomed. Anal. 25, 299–307.
Garg, A., Kokkoli, E., 2005. Characterizing particulate drug-delivery carriers with atomic force microscopy. IEEE Eng. Med. Biol. Mag. 24, 87–95.
Girardot, D., Jover, B., Moles, J.P., Deblois, D., Moreau, P., 2004. Chronic nitric oxide synthase inhibition prevents new coronary capillary generation. J. Cardiovasc. Pharmacol. 44, 322–328.
Gref, R., Quellec, P., Sanchez, A., Calvo, P., Dellacherie, E., Alonso, M.J., 2001. Development and characterization of CyA-loaded poly(lactic)-poly(ethylene glycol) PEG micro and nanoparticles. Comparison with conventional PLA particle carriers. Eur. J. Pharm. Biopharm. 51, 111–118.
Gupte, A., Nagarajan, R., Kilara, A., 1991. Block copolymer microdomains: a novel medium for enzymatic reactions. Biotechnol. Prog. 7, 348–354.
Hammady, T., Nadeau, V., Hildgen, P., 2006. Microemulsion and diafiltration approaches: an attempt to maximize the global yield of DNA-loaded nanospheres. Eur. J. Pharm. Biopharm. 62, 143–154.
Hombreiro Pérez, M., Zinutti, C., Lamprecht, A., Ubrich, N., Astier, A., Hoffman, M., Bodmeier, R., Maincent, P., 2000. The preparation and evaluation of poly(epsilon-caprolactone) microparticles containing both a lipophilic and a hydrophilic drug. J. Control. Release 65, 429–438.
Huang, Y.Y., Chung, T.W., 2001. Microencapsulation of gentamicin in biodegradable PLA and/or PLA/PEG copolymer. J. Microencapsul. 18, 457–465.
Ioele, G., Cione, E., Risoli, A., Genchi, G., Ragno, G., 2005. Accelerated photostability study of tretinoin and isotretinoin in liposome formulations. Int. J. Pharm. 293, 251–260.
Iwata, M., Nakamura, Y., McGinity, J.W., 1999. Particle size and loading efficiency of poly(D,L-lactic-co-glycolic acid) multiphase microspheres containing water soluble substances prepared by the hydrous and anhydrous solvent evaporation methods. J. Microencapsul. 16, 49–58.
Jenning, V., Golan, S.H., 2001. Encapsulation of retinoids in solid lipid nanoparticles (SLN). J. Microencapsul. 18, 149–158.
Jeong, J.C., Lee, J., Cho, K., 2003. Effects of crystalline microstructure on drug release behavior of poly(e-caprolactone) microspheres. J. Control. Release 92, 249–258.

Kikkinides, E.S., Charalambopoulou, G.C., Stubos, A.K., Kanellopoulos, N.K., Varelas, C.G., Steiner, C.A., 1998. A two-phase model for controlled drug release from biphasic polymer hydrogels. J. Control. Release 51, 313–325.
Lengsfeld, C.S., Manning, M.C., Randolph, T.W., 2002. Encapsulating DNA within biodegradable polymeric microparticles. Curr. Pharm. Biotechnol. 3, 227–235.
Lin, L.M., Li, B.X., Xiao, J.B., Lin, D.H., Yang, B.F., 2005. Synergistic effect of all-trans-retinoic acid and arsenic trioxide on growth inhibition and apoptosis in human hepatoma, breast cancer, and lung cancer cells in vitro. World J. Gastroenterol. 11, 5633–5637.
Mabrouk, M.M., el-Fatatry, H.M., Hammad, S., Wahbi, A.A., 2003. Simultaneous determination of loratadine and pseudoephedrine sulfate in pharmaceutical formulation by RP-LC and derivative spectrophotometry. J. Pharm. Biomed. Anal. 33, 597–604.
Muindi, J.R., Frankel, S.R., Huselton, C., DeGrazia, F., Garland, W.A., Young, C.W., Warrell Jr., R.P., 1992. Clinical pharmacology of oral all-trans retinoic acid in patients with acute promyelocytic leukemia. Cancer Res. 52, 2138–2142.
Nkansah, M.K., Tzeng, S.Y., Holdt, A.M., Lavik, E.B., 2008. Poly(lactic-co-glycolic acid) nanospheres and microspheres for short- and long-term delivery of bioactive ciliary neurotrophic factor. Biotechnol. Bioeng. 100, 1010–1019.
Panoyan, A., Quesnel, R., Hildgen, P., 2003. Injectable nanospheres from a novel multiblock copolymer: cytocompatibility, degradation and in vitro release studies. J. Microencapsul. 20, 745–758.
Panyam, J., Labhasetwar, V., 2003. Biodegradable nanoparticles for drug and gene delivery to cells and tissue. Adv. Drug Deliv. Rev. 55, 329–347.
Petrov, O., Furó, I., Schuleit, M., Domanig, R., Plunkett, M., Daicic, J., 2006. Pore size distributions of biodegradable polymer microparticles in aqueous environments measured by NMR cryoporometry. Int. J. Pharm. 309, 157–162.
Pistel, K.F., Breitenbach, A., Zange-Volland, R., Kissel, T., 2001. Brush-like branched biodegradable polyesters, Part III. Protein release from microspheres of poly(vinyl alcohol)-graft-poly(D,L-lactic-co-glycolic acid). J. Control. Release 73, 7–20.
Pistel, K.F., Kissel, T., 2000. Effects of salt addition on the microencapsulation of proteins using w/o/w double emulsion technique. J. Microencapsul. 17, 467–483.
Quesnel, R., Hildgen, P., 2005. Synthesis of PLA-b-PEG multiblock copolymers for stealth drug carrier preparation. Molecules 10, 98–104.
Rengarajan, K., Cristol, S.M., Mehta, M., Nickerson, J.M., 2002. Quantifying DNA concentrations using fluorometry: a comparison of fluorophores. Mol. Vis. 8, 416–421.
Rizkalla, N., Range, C., LaCasse, F.X., Hildgen, P., 2006. Effect of various formulation parameters on the properties of polymeric nanoparticles prepared by the multiple emulsion method. J. Microencapsul. 23, 39–57.
Ruan, G., Ng, J.K., Feng, S.S., 2004. Effects of polymer, organic solvent and mixing strength on integrity of proteins and liposomes encapsulated in polymeric microspheres fabricated by the double emulsion process. J. Microencapsul. 21, 399–412.
Sant, S., Thommes, M., Hildgen, P., 2008. Microporous structure and drug release kinetics of polymeric nanoparticles. Langmuir 24, 280–287.
Sinha, V.R., Bansal, K., Kaushik, R., Kumira, R., Trehan, A., 2004. Poly-ε-caprolactone microspheres and nanospheres: an overview. Int. J. Pharm. 278, 1–23.
Stafford, J.M., Elasy, T., 2007. Treatment update: thiazolidinediones in combination with metformin for the treatment of type 2 diabetes. Vasc. Health Risk Manag. 3, 503–510.
Strober, B.E., Clarke, S., 2004. Etanercept for the treatment of psoriasis: combination therapy with other modalities. J. Drugs Dermatol. 3, 270–272.
Sunderland, C.J., Steiert, M., Talmadge, J.E., Derfus, A.M., Barry, S.E., 2006. Targeted nanoparticles for detecting and treating cancer. Drug Dev. Res. 67, 70–93.
Tashtoush, B.M., Jacobson, E.L., Jacobson, M.K., 2008. UVA is the major contributor to the photodegradation of tretinoin and isotretinoin: implications for development of improved pharmaceutical formulations. Int. J. Pharm. 352, 123–128.
Wallace, D.G., Rosenblatt, J., 2003. Collagen gel systems for sustained delivery and tissue engineering. Adv. Drug Deliv. Rev. 55, 1631–1649.
Yang, Y.Y., Wan, J.P., Chung, T.S., Pallathadka, P.K., Ng, S., Heller, J., 2001. POE–PEG–POE triblock copolymer microspheres containing protein. I. Preparation and characterization. J. Control. Release 75, 115–128.